Post Print Applied Surface Science579(2022)152136

https://doi.org/10.1016/j.apsusc.2021.152136

Temperature and time dependent electron trapping in Al_2O_3 thin films onto AlGaN/GaN heterostructures

Patrick Fiorenza [(*)1], Emanuela Schilirò[1], Giuseppe Greco[1], Marilena Vivona[1], Marco Cannas[2], Filippo Giannazzo[1], Raffaella Lo Nigro[1] and Fabrizio Roccaforte[1]

[1]*Consiglio Nazionale delle Ricerche – Istituto per la Microelettronica e Microsistemi (CNR-IMM), Strada VIII, 5 - Zona Industriale, 95121 Catania Italy.*

[2]*Department of Physics and Chemistry Emilio Segre', University of Palermo, Via Archirafi 36, 90123 Palermo, Italy*

Abstract

In this article, the charge trapping phenomena in Al_2O_3 thin films grown by atomic layer deposition (ALD) on AlGaN/GaN heterostructures have been studied by time-dependent capacitance-voltage (C-V) measurements as a function of temperature. In particular, monitoring the transient of the capacitance enabled us to estimate the maximum depth of the insulating layer interested by the negative charge trapping effect under our bias stress conditions and to determine a charge traps density in the bulk Al_2O_3 in the order of 3×10^{19} cm^{-3}. A temperature dependent C-V analysis up to 150°C demonstrated the presence of two competitive mechanisms that rule the electron capture and emission in the Al_2O_3 film, characterized by activations energies of 22 and 88 meV respectively. Photoluminescence analyses revealed the presence of oxygen-related point defects in the insulator with a concentration in the order of $\sim10^{20}$ cm^{-3} envisaging that only a fraction of them is electrically active. The results are useful to establish the thermal stability of the trapping phenomena, and the possible application in real devices.

Keywords: Al_2O_3, Gallium Nitride, Plasma Enhanced Atomic Layer Deposition, charge trapping, capacitance transient measurements

[(*)] Corresponding Author: patrick.fiorenza@imm.cnr.it

INTRODUCTION

Aluminum oxide (Al_2O_3) is theoretically one of the most attracting insulating materials for a variety of applications in electronic devices [1]. In particular, thin Al_2O_3 layers can be used as gate insulator to reduce the leakage current in gallium nitride (GaN) high electron mobility transistors (HEMTs), and/or as passivation layer to reduce the current collapse phenomena [2,3]. The great interest towards Al_2O_3 thin films in GaN technology arises from its relevant electronic properties, e.g. the high relative dielectric permittivity κ (~ 9), the high critical electric field (10 MV/cm), the large band gap (~8.9) and the favorable band alignment with GaN [4].

Atomic Layer Deposition (ALD), either in thermal or plasma-enhanced mode, is certainly the most widely used technique to deposit Al_2O_3 thin films on GaN-based heterostructures [5]. In fact, ALD allows an accurate control of the deposition parameters inducing a self-limited growth mechanism, the control of film thickness and interface abruptness, and an uniform coverage at low deposition temperature, i.e. compatible with GaN thermal stability range and typical device processing temperatures [4]. However, the amorphous films grown by ALD are often characterized by the occurrence of negative charge trapping effects, especially when subjected to current or bias stress [6,7]. In particular, it is continuously debated that Al_2O_3 layers suffer by the presence of native defects [8,9,10] that influence the electrical behavior (i.e. leakage current) by introducing electronic levels in the band gap [11,12].

While the majority of the literature on GaN-based devices has been focused on the electrical properties of thermal ALD Al_2O_3 films [2,3,4,13,14,15], plasma-enhanced atomic layer deposition (PE-ALD) has been less explored in spite of its potential benefits with respect to the standard thermal ALD approach, e.g. the possibility to achieve a high growth rate and an improved film density at low deposition temperature [16,17]. However, independently of the deposition method, the mechanisms ruling the charge trapping in the bulk ALD Al_2O_3 films grown on GaN-based heterostructures have not been yet clarified [18,19]. In this context, some works have been devoted

to the theoretical comprehension of the impact of distributed bulk traps in ALD Al_2O_3 films on semiconductor compounds such as InGaAs [20], GaN [21] and AlGaN [22,23] on the threshold voltage stability of transistors. However, an experimental method to determine the amount of these traps in the insulator layer volume is missing. Furthermore, the knowledge of the charge/discharge phenomena occurring in bulk traps in ALD Al_2O_3 films is required to ultimately understand the possible impact on the power electronics device fabrication.

In the present paper, electron trapping/detrapping phenomena in bulk Al_2O_3 thin films deposited by PE-ALD on AlGaN/GaN heterostructures have been investigated by means of transient capacitance measurements and cyclic gate bias stress acquired at different temperatures. In particular, the temperature dependent cyclic gate bias stress allowed to determine the residual amount of charged bulk traps, while transient capacitance measurements allowed to estimate the maximum distance from the Al_2O_3/AlGaN interface of the bulk traps stimulated under our bias stress conditions. Insights on the optical emission properties of these bulk traps have been investigated also by means of photoluminescence measurements. Moreover, the stability of the enhancement mode operation in AlGaN/GaN MISHEMTs has been discussed in terms of the thermal emission of the bulk traps in Al_2O_3.

EXPERIMENTAL

The AlGaN/GaN heterostructures used in this study were grown on Si (111) substrates. The thickness of the AlGaN barrier layer was 16 nm, while the Aluminum concentration was 26% [19].

Al_2O_3/AlGaN/GaN circular MIS-capacitor and MISHEMTs were fabricated to monitor the electrical quality of the bulk oxide and of the interface, using the following procedure. First, the AlGaN surface has been cleaned using piranha (H_2O_2:H_2SO_4 =1:5) and diluted hydrofluoric acid (H_2O:HF=10:1) solutions, for 10 and 5 minutes, respectively [24,25]. Then the Ohmic contacts have been formed by a Ti/Al/Ni/Au multilayer annealed at 850°C [26]. Afterward, a 30nm thick

Al_2O_3 film has been deposited at 250°C using a PE-ALD LL reactor from SENTECH Instruments GmbH. Trimethyl-aluminum (TMA) and O_2-plasma were used as aluminum and oxygen sources, respectively. For the plasma-enhanced ALD mode, a 100 sccm O_2 flow was released to plasma source, while nitrogen (N_2), with a flow rate of 40sccm, has been used as carrier gas for TMA precursor. The pressure was 20 Pa during deposition. Finally, a gate contact consisting of a Ni/Au bilayer was defined by photolithography and lift-off [27]. The MISHEMT dimensions are gate-width of 200 µm and gate-length of 14 µm.

Time resolved photoluminescence (PL) spectra were excited by 5.85 eV-laser radiation generated in a pulsed tunable laser system (VIBRANT OPOTEK), pulse width ≈5 ns, repetition rate 10 Hz. The sample was excited by a laser beam, spot size of 3 mm, in 45° front-scattering geometry; the fluence/pulse, monitored with a pyroelectric detector, was fixed at 1 mJ/cm^2. The emitted light was spectrally resolved by a monochromator equipped with a 150 grooves/mm grating blazed at 300 nm, and then acquired by an intensified charge coupled device camera (PIMAX Princeton Instruments), setting the acquisition time window, T_W, and the delay, T_D, with respect to the arrival of excitation laser pulses. All the emission spectra were detected with a bandwidth of 3 nm and corrected for the instrumental response.

The test devices characterized by low frequency (1 kHz) capacitance-voltage (C-V) and current-voltage (I-V) measurements under different bias stress conditions. The C-V and I-V measurements on capacitors and transistors were carried out using a Microtech Cascade probe station equipped with a Keysight B1505 parameter analyzer varying the temperature between 25 and 150 °C. Atomic force microscopy (AFM) was carried out to investigate the surface morphology of the samples during the fabrication steps, using a Veeco Dimension 3100 AFM with a NanoScope V controller. Transmission electron microscopy (HR-TEM) on cross-section samples enabled us to monitor the structural quality of the Al_2O_3/AlGaN interface.

RESULTS AND DISCUSSION

Morphological, structural and chemical properties

The investigation started from the morphological, structural and chemical points of view. Figs. 1a and 1b show the AFM morphology collected on the AlGaN/GaN and Al_2O_3/AlGaN/GaN surfaces, respectively. The heights distribution collected on the scanned area can be visualized as shown in Fig. 1c. Fig. 1c shows also the comparison between the heights distribution collected both on the Al_2O_3 and on the AlGaN/GaN substrate bare surfaces. As can be seen, very smooth surface of the deposited Al_2O_3 film is achieved. Furthermore, Figs. 1d and 1e report the cross-sectional TEM micrographs showing the abrupt Al_2O_3/AlGaN interface between the amorphous insulator and the crystalline semiconductor substrate.

Often, the Al_2O_3/AlGaN/GaN system is used to fabricate MISHEMTs with a tunable threshold voltage (V_{th}). In fact, MISHEMTs having a $V_{th} < 0$ V due to the active presence of a 2DEG in the gate region – namely called "normally- on" transistors – can become "normally-off" after the suppression of the 2DEG in the gate region by an appropriate positive gate bias stress procedure [7]. In particular, electrons trapped in the gate region produce an electrostatic repulsion on the 2DEG inhibiting the conduction between source and drain.

Johnson et al. [28] and *Hou et al.* [29] observed an analogous trapping effect in HfO_2 and Al_2O_3 AlGaN/GaN MISHEMTs and attributed it to the presence of a GaON interfacial layer formed during the thermal ALD process. However, our TEM analyses did not reveal the presence of such interfacial layer.

On the other hand, a chemical analysis based on electron energy-loss spectroscopy performed on amorphous Al_2O_3 films grown under the same conditions showed the presence of low coordinated Al cations in the layers, which is an indication of oxygen vacancies [7]. However, a

clear identification of the electrically active defects in the amorphous Al_2O_3 film is not yet provided.

Figs. 2a and 2b report the PL spectra in the 2.0-4.0 eV range of the AlGaN/GaN and Al_2O_3/AlGaN/GaN samples, respectively, acquired under excitation at 5.85 eV with T_W=10 ns and T_D=6 ns. While in the UV region both samples emit a peak centered around 3.4 eV, well associated with the GaN band gap transition [30], different features are observed in the visible. Indeed, the Al_2O_3/AlGaN/GaN exhibits a band peaked at 2.9 eV with full width half maximum (FWHM) ≈0.5 eV (Fig. 2b), that decays in few ns. This emission certainly originates from point defects in the Al_2O_3 layer, their concentration can be roughly estimate of the order of ~10^{20} cm^{-3} by comparing the PL amplitude with that measured in a reference sample containing a known concentration of luminescent defects, nonbridging oxygen hole centers in irradiated silica [31], normalizing appropriately for the excited volume. It is worth noting that in earlier works [9], Perevalov et al. recorded a PL band at 2.9 eV in amorphous Al_2O_3 films, ~ 20 nm thick, with excitation and decay characteristics similar to those observed in the present work. Those authors associated this emission with oxygen vacancies and measured a concentration of N≈7×10^{20} cm^{-3}.

Electrical properties

The electrical characterization is carried out in order to fully investigate the effects of temperature and time on the charge trapping effects in Al_2O_3/AlGaN/GaN system. In particular, the electrical characterization of the Al_2O_3/AlGaN system started with a method to separate the trapping phenomena both at the interface and inside the insulating layer.

Firstly, the trapping phenomena have been investigated on Al_2O_3/AlGaN/GaN MIS capacitors, by the C-V measurements, reported in Fig. 3 at different tempatures (25 °C (a,b,c, and d); 75 °C (3); 125 °C (f)). In particular, C–V curves have been collected by increasing the final positive gate bias stress from 0 V up to + 14 V with + 2 V steps.

To avoid an underestimation of the trapping phenomena, as may occur in AlGaN/GaN MISHEMTs probed by high-frequency C-V measurements [32,33], our C-V measurements have been carried out at 1kHz

In the C-V characterization reported in the following part, the gate bias was swept from negative toward positive values (from depletion to accumulation) and backward from positive toward negative biases (from accumulation to depletion). The cyclic C-V curves have been sequentially collected by increasing the final gate bias value by + 2 V from 0V to +14V on "fresh" (i.e. non-stressed) MIS capacitors. The hysteresis between the forward and backward C-V curves in two different specific regions has been recorded for different gate bias stress conditions. This procedure allowed to discriminate among the different trapping contributions at the Al_2O_3/AlGaN interface and inside the insulator.

The first C-V measurement (Fig. 3a), collected from V_G = – 10V to 0V and backward, shows no hysteresis. This means that the depletion of the two dimensional electron gas (2DEG) at the AlGaN/GaN interface occurs at the expected "pinch-off" bias value V_{PO}= – 7.5 V [34].

Further cyclic C-V curves acquired by increasing the final positive gate bias stress value by steps of +2 V up to the final value of+14V have been collected (Figs. 3b, 3c, and 3d). During this progressive cyclic gate bias stress procedure, it is possible to monitor both the pinch-off bias V_{PO} (Fig. 3 a) and the "*flat band voltage*" V_{FB} (Fig. 3b), this latter defined as the point of the intersection of the second derivative of the C-V curve with the positive gate bias axis region [35]. In fact, for positive gate bias values, the C-V curves starts exhibiting a second step due to accumulation of electrons in the AlGaN layer at the Al_2O_3 interface that can be monitored by the V_{FB} shifts.

These hystereses can be attributed to different charge trapping phenomena occurring in the MIS system. In particular, the flat band voltage shift ΔV_{FB} is associated with the charging of the Al_2O_3/AlGaN interface states. On the other hand, the pinch-off bias shift ΔV_{PO} is due to the charge trapping in the bulk Al_2O_3 film [36]. Similarly, Figs. 3e and 3f show the hysteresis between the forward and backward C-V curves collected at 75 °C and 125 °C, respectively. As discusses later

in the paper, a more detailed analysis of these cyclic C-V curves collected at different temperatures enabled to get determine the termperature-dependent charge trapping behaviour.

An additional analysis of the cyclic C-V curves allowed us to determine the charge traps density and their location inside the insulator.

According to the planar capacitor approximation, the total amount of charge trapped at the Al_2O_3/AlGaN interface (N_{it}) can be obtained by:

$$N_{it} = \frac{\Delta V_{FB} C_{Al_2O_3}}{q} \quad (1)$$

where $C_{Al_2O_3}$ is the insulator layer capacitance in accumulation and q is the electron charge.

In a similar way, the capacitance plateaux C_{PO} observed close to V_G = 0 V is the series of the insulator ($C_{Al_2O_3}$) and AlGaN layer (C_{AlGaN}) capacitances and can be used to extract the total amount of charge trapped at the Al_2O_3 bulk interface (N_{OT}):

$$N_{OT} = \frac{\Delta V_{PO}\left(\frac{t_{Al_2O_3}}{\kappa_{Al_2O_3}\varepsilon_0}+\frac{t_{AlGaN}}{\kappa_{AlGaN}\varepsilon_0}\right)^{-1}}{q} \quad (2)$$

where $t_{Al_2O_3}$ and t_{AlGaN} are the Al_2O_3 and AlGaN layer thicknesses, while $\kappa_{Al_2O_3}$ and κ_{AlGaN} are the Al_2O_3 and AlGaN relative dielectric permittivities.

Fig. 4 reports the ΔV_{FB} (a) and ΔV_{PO} (b) shifts that are due to the total amount of the trapped charges at the Al_2O_3/AlGaN interface (N_{it}) and in the bulk Al_2O_3 (N_{OT}), respectively. The values are collected as a function of the positive value of the final gate bias stress, at the different measurement temperatures from 25°C to 150 °C.

The values of the trapped charges have been extracted from the C-V curves from the shifts ΔV_{FB} and ΔV_{PO}, using Eq. (1) and Eq. (2), respectively. As it can be seen, at all the measurement temperatures the values of ΔV_{FB} (red curves in Fig. 5a) after an increase below 6V tend to saturate at high stress bias to a value of interface trapped charge N_{it}= 7×10^{12} cm^{-2} (see Fig. 5a). On the

other hand, the positive ΔV_{PO} shift does not show a saturation with increasing the bias stress or a monotronic trend with increasing the temperature (Fig. 4b).

It must be pointed out that an analogous trapping behavior has been observed in Al_2O_3 films deposited on 4H-SiC under similar conditions [37]. This latter allows us to rule out an effect of the GaN buffer, as observed by other authors under reverse bias [38,39].

In order to get further insights on the trapping phenomena and on the stability of the enancement mode MISHEMT behavior, a temperature dependence of the transfer characteristics after bias stress has been carried out.

Fig. 5a reports a series of sequential transfer characteristics (I_D-V_G) of the Al_2O_3/AlGaN/GaN MISHEMT after a +14 V positive gate bias stress, collected sweeping the gate bias from a large negative bias (i.e. V_G = - 20 V) up to a moderate positive gate bias (i.e. V_G = + 5 V) at 100 °C following the green arrow direction (Fig. 5a) and at 150°C (Fig. 4b).

The V_D = 0.1 V value has been chosen not only to minimize the self heating effect but also to get information on the turn-on process of the HEMT keeping a low perturbation of the Al_2O_3 traps.

As can be noticed, after the positive gate bias the MISHEMT shows an enhancement-mode behavior, with a positive pinch-off bias V_{PO}=+1.5 V.

Fig. 5c reports the device pinch-off bias V_{PO} measured during the sequence of several transfer characteristics of the device collected at 100°C between V_G =– 20V to +5V depicted in Fig. 5a. Evidently, the device shows only a small variation of the V_{PO}, i.e. the enhancement mode operation is preserved. On the other hand, the same sequence at 150°C (Fig. 5b) leads to a more significant variation of the V_{PO}, which reach the zero (V_{PO}=0V) after 6 sweeps. An additional increase of the negative bias stress, by means of an increased number of the gate ramps, induced a further shift of V_{PO} toward negative values, which indicates that the ehnanced-mode operation is not anymore stable at 150 °C.

Noteworthy, the V_{PO} stability depends on the temperature and the reverse biasing that promotes the electron emission from the Al_2O_3 traps. Hence, our results are a "proof of concept" of the possibility to control the electron trapping in a specific region of the device.

In order to estimate the amount of bulk traps per volume unit in the insulator, it is needed the estimation of the insulator volume fraction involved in the mentioned trapping phenomenon under our experimental conditions of bias stress. Hence, it is mandatory to determine the depth of the charged bulk traps from the Al_2O_3/AlGaN interface. It is believed that the trapping phenomena have a time-dependent behaviour depending on several parameters.

According to *Fujino and Kita* [40], the trapping/detrapping of the near-interface-oxide-traps (NIOTs) in MOS capacitors produces a transient capacitance *C(t)* variation. This transient capacitance can be described by the so called "*extended-Debye relaxation model*" [41] instead of a conventional relaxation model with a single time constant using the equation:

$$\Delta C \equiv \left[C(t) - C_{eq}\right] \cong |\Delta C_0| exp\left\{-\left(\frac{t}{\tau_{eff}}\right)^{\beta}\right\} \quad (3)$$

where *C(t)* is the capacitance at each time, C_{eq} is the capacitance at the equilibrium (i.e, after 1000s in our case), τ_{eff} is the characteristic tunneling time needed for the carrier transport back and forth from the NIOTs, ΔC_0 is the total change of capacitance caused by the detrapping of NIOTs and the semiconductor and $0<\beta<1$ is a fitting parameter [42]. Indeed, the characteristic tunneling time τ_{eff} is related to the spatial location of the NIOTs with respect to the insulator/semiconductor interface.

The charge penetration distance from the semiconductor into the insulator depends on the applied electric field and stress duration time [43]. In fact, it can be assumed that for a single trap energy and uniform spatial distribution of traps in the insulator the tunneling injection from the semiconductor into the insulator is always sharply peaked spatially. Furthermore, this peak moves at a linear-with-log-time rate of about 2 Å per decade of time into the insulator, giving rise to the notion of a tunneling front [43]. Hence, the variation of the gate bias stress condition in the

capacitance transient measurement may help to understand which is the deepest trap reached inside the insulator during the charge injection. In fact, the deepest trap reached inside the insulator during the charge injection is the slowest trap to be stimulated.

The experimental relaxation time can be used to estimate the maximum distance (x) from the insulator/semiconductor interface that is interested, in our experimental stress conditions, by the trapping/detrapping phenomenon.

Paulsen et al. [44] described the relaxation time $\tau(x)$ of a δ-shaped distribution of traps located at a distance x from the semiconductor interface using the following equations:

$$\tau(x) = \frac{m_1^* x\left(1+\frac{1}{2\eta_1 x}\right)}{2\pi\eta_2\hbar^3 D_{it}} exp(2\eta_1 x) \quad (4)$$

where

$$\eta_1^2 = \frac{2m_1^*\left(\phi_B + E_C - E_f\right)}{\hbar^2} \quad (5)$$

and

$$\eta_2^2 = \frac{2m_2^*\left(E_C - E_f\right)}{\hbar^2} \quad (6)$$

where ϕ_B is the energy discontinuity between the semiconductor and the oxide, m_1* and m_2* are the effective masses for electrons in the oxide and semiconductor respectively, and E_f, is the position of the Fermi level in the semiconductor. Furthermore, D_{it} is the interface state density close to the AlGaN conduction band edge, $\hbar$ is the reduced Plank constant. Considering that the transient characterization is carried out in strong accumulation, the E_f position can be considered as the energy position of the trap level inside the insulator. The transient is collected in strong accumulation, E_f position coincides with the AlGaN conduction band edge and it gives information on the energetic location of the Al_2O_3 trats within its band gap.

Fig. 6a shows the experimental transient capacitance $\Delta C/\Delta C_0$ collected at room temperature used to be fitted using Eq. 3 to extract the effetive relaxation time $\tau_{eff} \approx 28$ s. Furthermore, Fig. 6a shows that incresing the gate bias stress condition (i.e. from V_G = + 7.5 V up to V_G = + 10 V) the

effetive relaxation time is not varied demonstrating that the injected charge cannot reach any physical position inside the insulating layer. The inset of Fig. 6a shows the exponential decay of the capacitance in good agreement to Eq. 3

Eq. 4 is solved considering the literature values of m_1* and m_2* [45,46] as a function of the distance *x* between the deepest bulk trap and the Al_2O_3/AlGaN interface, as shown in Fig. 6b. To solve Eq. 4 realistic D_{it} values are used ranging between 10^{12} up to 10^{14} $cm^{-2}eV^{-1}$. However, this produces an extrapolation error of a less than one Ångström around the mean value of 1.5 nm (see Fig. 6b). The depth of 1.5 nm can be considered as the location of the deepest trap in the insulator determining the transient capacitance behavior observed under our stress conditions. While *Matys et al.* [22] reported about a simulated spatial extension of traps into the dielectric bulk about 4 nm from the insulator/semiconductor interface in ALD Al_2O_3/AlGaN system to fit their results, in our case the electron penetration is limited within a narrow region of the insulator close to the semiconductor interface.

The spatial estention of the detected bulk traps from the Al_2O_3/AlGaN interface is an information needed to convert the amount of traps in the volume fraction from the surface density determined from the ΔV_{PO} shifts. From Fig. 4b and Fig. 6b it is possibile to determine the amount of traps in the volume fraction (about 1.5 nm from the semiconductor interface) of the insulator interested by the trapping/detrapping phenomena of $N_{bulk} \approx 3\times10^{19}$ cm^{-3}. This is one order of magnitude lower trap concentration compared to the believed and detected by PL oxygen vacancies concenteration [9]. Hence, it is possible to argue that only a part of the oxygen-related defects is actually active as an electron trap or on another hand, the total amount of the F-centers is lower than argued from the PL analysis.

As can be seen in Fig. 4b, the increasing rate of the ΔV_{PO} measured with increasing the positive gate bias stress (i.e. V_G = + 14 V) has different behaviors at different temperatures. This means that the larger the positive gate bias stress is the deeper bulk trap can be reached. In particular, it can be noticed that increasing the temperature the gate bias stress curves show a different growing

behavior with a concavity change above 100 °C. This result can be analyzed and interpreted looking at the ΔV_{PO} measured at V_G = + 14 V at different temperatures, which is reported in an Arrhenius-like plot in Fig. 7.

As can be noticed in Fig. 7, the amount of the detected charged bulk traps first increases with increasing the gate bias stress temperature up to 100 °C, and then decreases upon a further increase of the temperature up to 150 °C. Hence, the presence of two competitive trap-assisted mechanisms is envisaged. In particular, it can be argued that one mechanism is favorable to the bulk trap filling – with an activation energy of E_A ~ 22 meV (with the assumption of $N_{OT} \propto \pm E_A/kT$) – dominating at low temperature, while a second mechanism promotes the electron emission from the traps states – with an activation energy of E_A ~ 88 meV – once the temperatue is raised.

Fig. 8 schematically illustrates the trapping/detrapping effect occurring near the Al_2O_3/AlGaN interface.

As mentioned before, by increasing the gate bias stress no charge deeper than 1.5 nm from the semiconductor interface is stimulated. However, by increasing the gate biasing one can ehnance the emission of the trapped charge in the insulator conduction band moving toward the metal gate.

CONCLUSION

The electron trapping occurring in the bulk of Al_2O_3 films grown by plasma enhanced atomic layer deposition on AlGaN/GaN heterostructures has been studied by means of time-dependent C-V characterizations at different temperatures. These characterizations allowed to determine the maximum depth of the insulating layer interested by a negative charge trapping effect and to determine the amount of volume charge traps in the bulk Al_2O_3 in the order of 3×10^{19} cm^{-3}. These electron bulk traps can be associated with a fraction of the oxygen vacancies revealed by PL measurements. Hence, only a fraction optically detected point defects is electrically active.

A temperature dependent C-V analysis demonstrated the presence of two competivive trap-assisted mechanisms that promote the electron capture and the emission in the Al_2O_3 film. These charge trapping effects are stable up to 100°C under reverse bias stress operation.

These results can be particularly useful for device manufacturers and open new routes for controlling the enhancement-mode operation in AlGaN/GaN MISHEMTs.

ACKNOWLEDMENTS

The authors would like to thank S. Di Franco and C. Bongiorno for technical assistance during device fabrication and TEM analyses, respectively. This work has been funded by the Italian Ministry for University and Research (MUR) in the framework of the National Project PON EleGaNTe (Electronics on GaN-based Technologies), ARS01_01007.

The data that support the findings of this study are available from the corresponding author upon reasonable request.

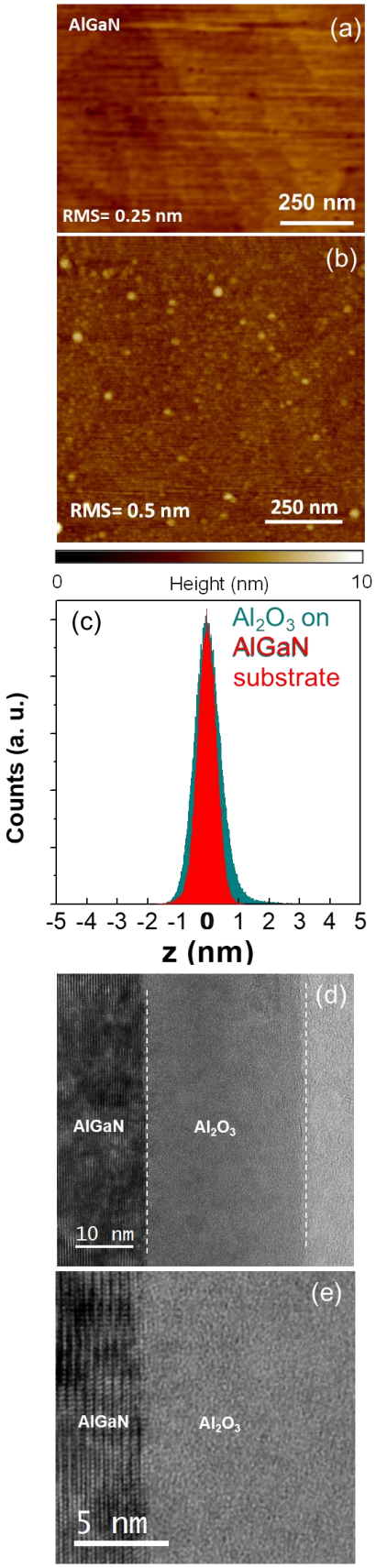

Fig. 1: (a) Morphological AFM image on the AlGaN/GaN and (b) Al_2O_3/AlGaN/GaN bare surfaces respectively. The heights distributions collected on the substrate and on the Al_2O_3 (c). Low and high resolution cross-sectional TEM image of the Al_2O_3/AlGaN interface (d) and (e) respectively.

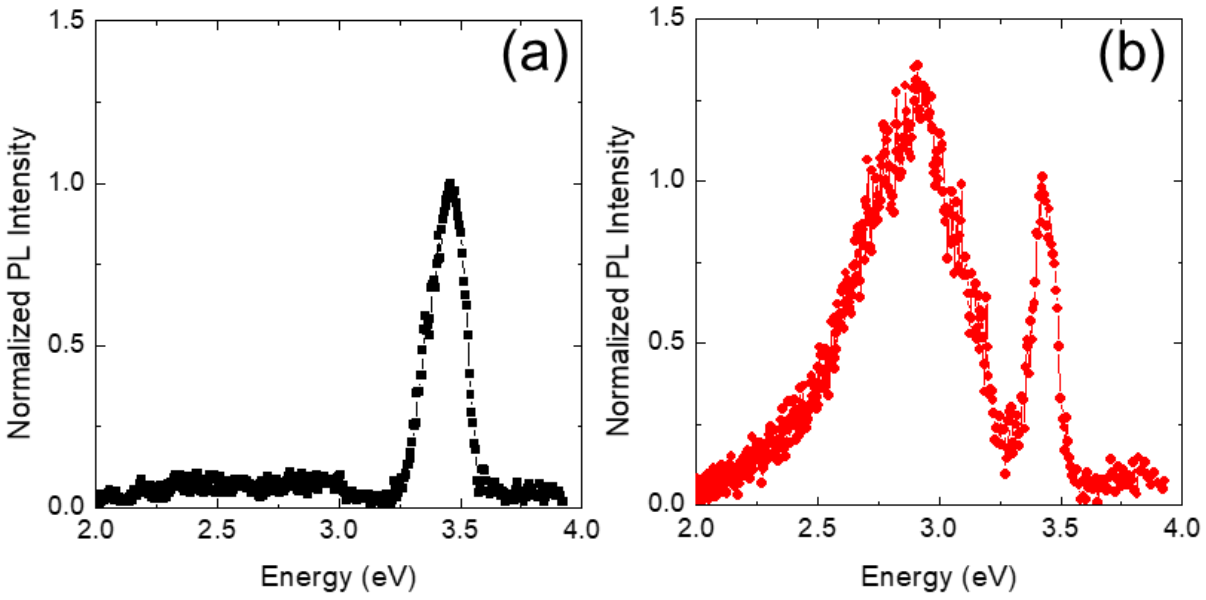

Fig. 2: PL-spectrum measured under laser excitation at 5.85 eV for (a) the AlGaN/GaN and (b) Al_2O_3/AlGaN/GaN sample.

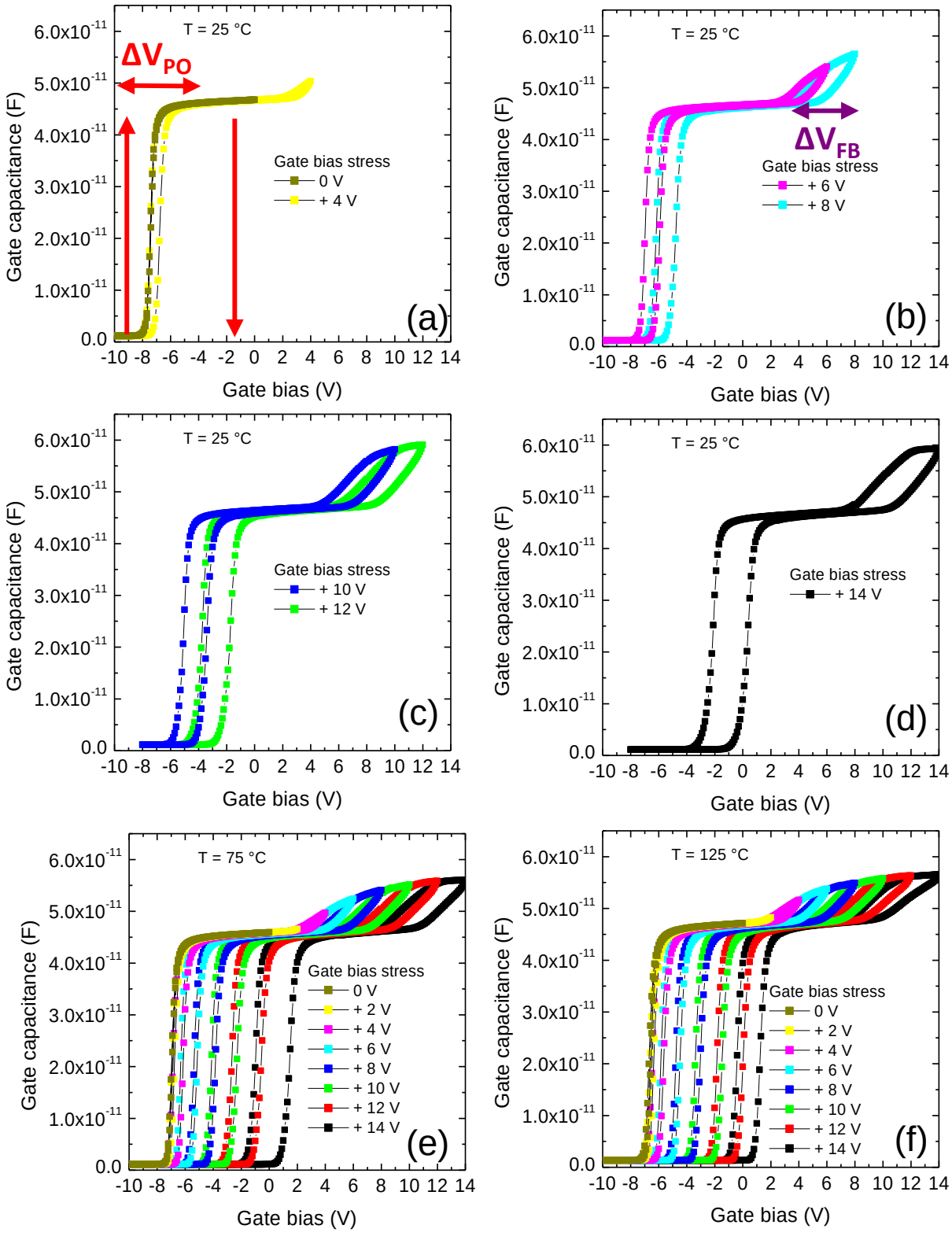

Fig. 3: C-V curves collected on an Al_2O_3/AlGaN/GaN MIS capacitor sweeping the gate bias from depletion-to-accumulation and backward, by increasing the final the gate bias value at different temperatures: 25 °C (a), 75 °C (b); and 125 °C (c).

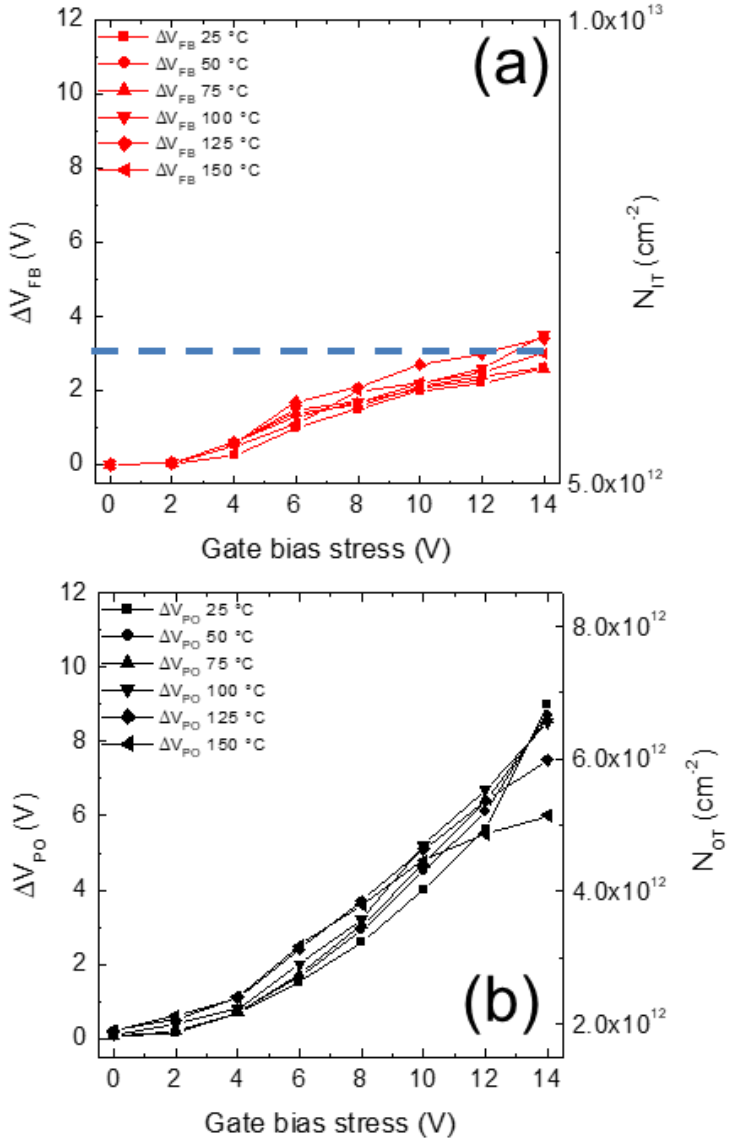

Fig. 4: Flat band voltage shift ΔV_{FB} (a) and pinch-off bias shift ΔV_{PO} (b) extracted from the cyclic C-V curves collected at temperatures form 25 up to 150 °C.

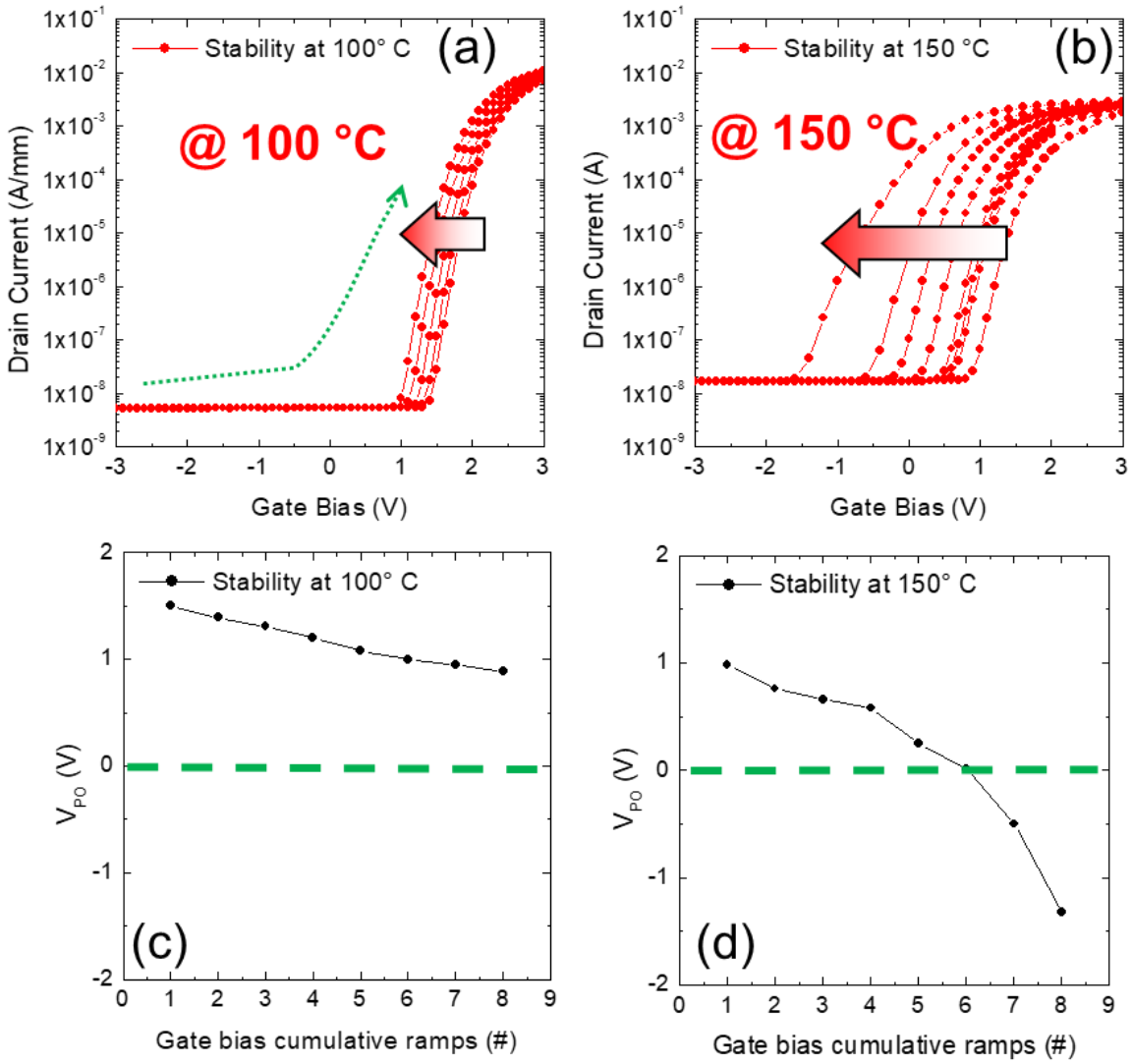

Fig. 5: (a) Series of 8 I_D-V_G characteristics collected at V_{DS}=0.1V for the Al_2O_3/AlGaN/GaN MISHEMT after gate bias stress at 14V collected at 100 °C (a) and at 150°C (b). Shift of the pinch-off ΔV_{PO} observed on the I_D-V_G characteristics after each ramp of stress, at 100 °C (c) and 150 °C (d).

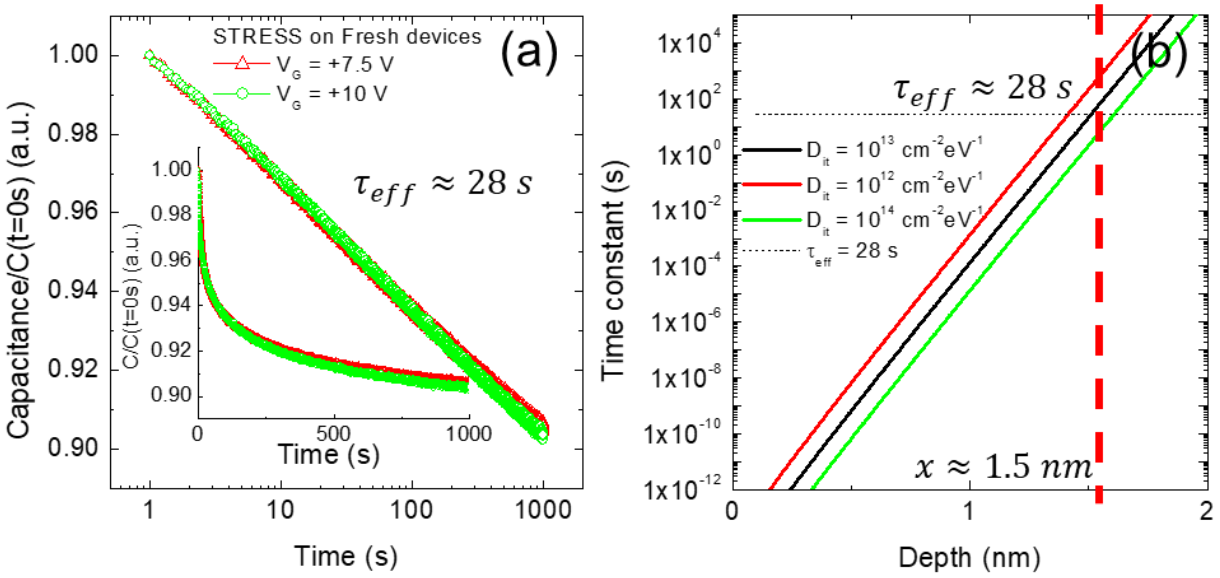

Fig. 6: (a) Experimental $\Delta C/\Delta C_0$ vs time acquired on Al_2O_3/AlGaN MIS capacitors subjected to two different gate bias stress of 7.5V and 10V. In the inset, the capacitance exponential decay is shown in linear time scale. (b) Time constant as a function of the depth between the bulk traps and the Al_2O_3/AlGaN interface, calculated using Eq. 4. The experimental value τ_{eff}=28s correspond to a depth x=1.5 nm.

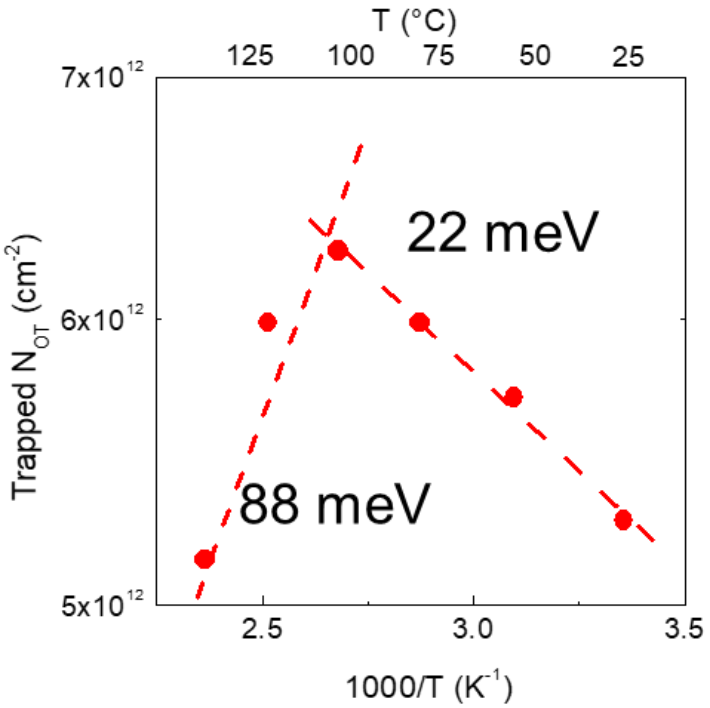

Fig. 7: Arrhenius plot of the trapped charge density determined from the ΔV_{PO} measured in Fig.2 at V_G = + 14 V.

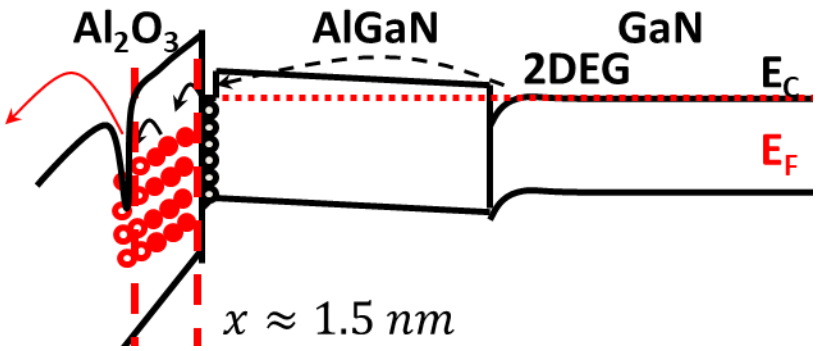

Fig. 8: Schematic energy band diagram of the Al_2O_3/AlGaN/GaN system at $V_G \gg 0$ V. The electron spill-over from the 2DEG is filling the bulk oxide traps at a distance of 1.5 nm from the semiconductor interface.

References

[1] G.D. Wilk, R.M. Wallace and J.M. Anthony, *J. Appl. Phys.* **89**, 5243-5275 (2001).
[2] F. Roccaforte, P. Fiorenza, G. Greco, M. Vivona, R. Lo Nigro, F. Giannazzo, A. Patti, M. Saggio, *Appl. Surf. Sci.* **301**, 9-18 (2014).
[3] T. Hashizume, K. Nishiguchi, S. Kaneki, J. Kuzmik, Z. Yatabe, *Mater. Sci. Semicond. Proc.* **78**, 85-95 (2018).
[4] F. Roccaforte, P. Fiorenza, R. Lo Nigro, F. Giannazzo, G. Greco, *Riv. Nuovo Cimento* **41**, 625-681 (2018).
[5] T. Kääriäinen, D. Cameron, M.-L. Kääriäinen and A. Sherman, *Atomic Layer Deposition, Principles Characteristics and Nanotechnolody applications* edited by M. Scrivener and P. Carmical (2013)
[6] S.-J. Park, J.-P. Lee, J. S. Jang, H. Rhu, H. Yu, B.Y. You, C.S. Kim, K.J. Kim, Y.J. Cho, S. Baik, W. Lee, *Nanotechnology* **24**, 295202 (2013).
[7] E. Schilirò, P. Fiorenza, C. Bongiorno, C. Spinella, S- Di Franco, G. Greco, R. Lo Nigro, F. Roccaforte, *AIP Advances* **10**, 125017 (2020).
[8] M. Choi, A. Janotti, C.G. Van de Walle, *J. Appl. Phys.* **113**, 044501 (2013).
[9] T.V. Perevalov, O.E. Tereshenko, V.A. Gritsenko, V.A. Pustovarov, A.P. Yelisseyev, C. Park, J. Hee Han, C.J. Lee, *J. Appl. Phys.* **108**, 013501 (2010).
[10] J. Robertson, *Solid-State Electronics* **49**, 283-293 (2005).
[11] D. Liu, S.J. Clark, J. Robertson, *Appl. Phys. Lett.* **96**, 032905 (2010).
[12] R. Weber, A. Janotti, C.G. Van de Walle, *J. Appl. Phys.* **109**, 033715 (2011).
[13] S. Ganguly, J. Verma, G. Li, T. Zimmermann, H. Xing, D. Jena, *Appl. Phys. Lett.* **99**, 193504 (2011).
[14] M. Esposto, S. Krishnamoorthy, D.N. Nath, S. Bajaj, T-H. Hung, S. Rajan, *Appl. Phys. Lett.* **99**, 133503 (2011).
[15] Y. Zhang, M. Sun, S.J. Joglekar, T. Fujishima, T. Palacios, *Appl. Phys. Lett.* **103**, 033524 (2013).
[16] H. Kim, I-K. Oh, *Jpn. J. Appl. Phys.* **53**, 03DA01 (2014).
[17] D.R. Boris, V.D. Wheeler, N. Nepal, S.B. Qadri, S.G. Walton, C.R. Eddy, *J. Vac. Sci. Technol. A* **38**, 040801 (2020).
[18] M. Tapajna, L. Valik, F. Gucmann, D. Gregusova, K. Froehlich, S. Hascık, E.Dobrocka, L. Tothand, B, Pecz, J. Kuzmık, *J. Vac. Sci. Technol. B* **35**, 01A107 (2017).
[19] P. Fiorenza, G. Greco, E. Schilirò, F. Iucolano, R. Lo Nigro, F. Roccaforte, *Jpn. J. Appl. Phys.* **57**, 050307 (2018).
[20]Y. Yuan, B. Yu, J. Ahn, P. C. McIntyre, P. M. Asbeck, M. J. W. Rodwell, Y. Taur; *IEEE Trans Electr Dev.* **59**, 2100 (2012)
[21] D. Bisi, S. H. Chan, X. Liu, R. Yeluri, S. Keller, M. Meneghini, G. Meneghesso, E. Zanoni, and U. K. Mishra, *Appl. Phys. Lett.* **108**, 112104 (2016).
[22] M. Matys, S. Kaneki, K. Nishiguchi, B. Adamowicz, and T. Hashizume, *J. Appl. Phys.* **122**, 224504 (2017).
[23] F. Roccaforte, G. Greco, P. Fiorenza, F. Iucolano; *Materials*, **12**, 1599 (2019)
[24] E. Schilirò, G. Greco, P. Fiorenza, C. Tudisco, G.G. Condorelli, S. Di Franco, F. Roccaforte, R. Lo Nigro, *Phys. Status Solidi C* **12**, 980-984 (2015).
[25] R. Lo Nigro, E. Schilirò G. Greco, P. Fiorenza, F. Roccaforte; *Thin Solid Films* **617**, 138 (2016)
[26] G. Greco, F. Iucolano, F. Roccaforte *Appl. Surf. Sci.* **383**, 324-345 (2016).
[27] G. Greco, F. Giannazzo, and F. Roccaforte, *J. Appl. Phys.* **121**, 045701 (2017).
[28] D. W. Johnson, R. T. P. Lee, R. J. W. Hill, M. H. Wong, G. Bersuker, E. L. Piner, P. D. Kirsch, and H. R. Harris, *IEEE Trans. Electron Devices* **60**, 3197–3203 (2013).

[29] B. Hou, X. Ma, J. Zhu, L. Yang, W. Chen, M. Mi, Q. Zhu, L. Chen, R. Zhang, M. Zhang, X. Zhou, and Y. Hao, *IEEE Electron Device Lett.* **39**, 397–400 (2018).
[30] F. Roccaforte, F. Giannazzo, A. Alberti, M. Spera, M. Cannas, I. Cora, B. Pécz, F. Iucolano, G. Greco; *Mater. Sci. Semicond. Process.* **94**, 164 (2019)
[31] L. Vaccaro, M. Cannas, B. Boizot, A. Parlato; *J. Non-Cryst. Solids* **353**, 586 (2007)
[32] W M. Waller, S. Karboyan, M. J. Uren, K. Boon Lee, P.A. Houston, D. J. Wallis, I. Guiney, C.J. Humphreys, M. Kuball; *IEEE Trans Electron Dev*, **62**, 2464 (2015)
[33] J. Osvald; *Physica E* **93**, 238-242 (2017)
[34] O. Ambacher, J. Smart, J.R. Shealy, N.G. Weimann, K. Chu, M. Murphy, W.J. Schaff, L.F. Eastman, R. Dimitrov, L. Wittmer, M. Stutzmann, W. Rieger, J. Hilsenbeck, *J. Appl. Phys.* **85**, 3222-3233 (1999).
[35] R. Winter, J. Ahn, P. C. McIntyre, M. Eizenberg J. Vacuum Sci. Tech. B 31, 030604 (2013)
[36] D.W. Johnson, R.T.P. Lee, R.J.W. Hill, M.H. Wong, G. Bersuker, E.L. Piner, P.D. Kirsch, H.R. Harris, *IEEE Transaction on Electron Devices* **60**, 3197-3203 (2013).
[37] E. Schilirò, R. Lo Nigro, P. Fiorenza, F. Roccaforte *AIP Advances* **6**, 075021 (2016)
[38] A. Pérez-Tomás, A. Fontserè, J. Llobet, M. Placidi, S. Rennesson, N. Baron, S. Chenot, J. C. Moreno, Y. Cordier, *J. Appl. Phys.* **113**, 174501, (2013)
[39] D. Bisi, M. Meneghini, F. A. Marino, D. Marcon, S. Stoffels, M. Van Hove, S. Decoutere, G. Meneghesso, E. Zanoni, *IEEE Electron Device Lett.* **35**, 1004 (2014).
[40]Y. Fujino, K. Kita, *ECS Transactions*, **69** 219-225 (2015)
[41] A. K. Jonscher *J. Phys. D*, **32**, R57 (1999)
[42] P. Fiorenza, F. Iucolano, G. Nicotra, C. Bongiorno, I. Deretzis, A. La Magna, F. Giannazzo, M. Saggio, C. Spinella, F. Roccaforte *Nanotechnology* **29** 395702 (2018)
[43] A.J. Lelis, R. Green, D.B. Habersat, M. El, *IEEE Trans. Electron Dev.* **62** 316 (2015).
[44] R. E. Paulsen, R. R. Siergiej, M. L. French, M. H. White, *IEEE Electr. Dev. Lett.*, **13**, 627 (1992)
[45] T. V. Perevalov, A. V. Shaposhnikov, V. A. Gritsenko, H. Wong, J. H. Han, C. W. Kim; *JETP Letters*, **85**, 165–168 (2007)
[46] T. Hofmann, P. Kühne, S. Schöche, Jr-Tai Chen, U. Forsberg, E. Janzén, N. Ben Sedrine, C. M. Herzinger, J. A. Woollam, M. Schubert, V. Darakchieva; *Appl. Phys. Lett.* **101**, 192102 (2012)